OPEN ACCESS
IOP Publishing
Superconductor Science and Technology
Supercond. Sci. Technol. **31** (2018) 105005 (9pp)
https://doi.org/10.1088/1361-6668/aad786

Exploiting flux jumps for pulsed field magnetisation

Difan Zhou[1,3], Mark D Ainslie[1], Jan Srpčič[1], Kaiyuan Huang[1], Yunhua Shi[1], Anthony R Dennis[1], David A Cardwell[1], John H Durrell[1], Martin Boll[2] and Mykhaylo Filipenko[2]

[1] Department of Engineering, University of Cambridge, Trumpington Street, Cambridge CB2 1PZ, United Kingdom
[2] Siemens AG Corporate Technology, Willy-Messerschmitt-Str. 1, D-82024 Taufkirchen, Germany

E-mail: dz286@cam.ac.uk

Received 8 June 2018, revised 19 July 2018
Accepted for publication 2 August 2018
Published 28 August 2018

Abstract

Magnetisation is one of the main barriers to practical use of bulk superconductors as high field magnets. Recently several authors have reported a flux jump effect that allows penetration of magnetic flux into a bulk superconductor during pulsed field magnetisation (PFM) at lower fields than that would be predicted on the basis of the Bean model. We have systematically investigated macroscopic flux jumps in single grain $GdBa_2Cu_3O_{7-\delta}$–Ag (GdBCO–Ag) bulk superconductors with diameters of up to 30 mm when subjected to pulsed magnetic fields. Flux jumps were observed at temperatures between 30 and 77 K and in applied magnetic fields of up to 7 T. The applied pulsed field required to trigger the instability or flux jump field, B_j, was determined experimentally and found to increase with decreasing temperature. An extended instability criterion based on a 2D axisymmetric model was used to predict B_j at various temperatures and the results are in good agreement with experiments. A significant temperature rise has been measured experimentally during the magnetisation process which indicates that local heat generation due to the sharp rise of the applied field in the PFM process is the primary cause of the flux jumps. The experimental results suggest further that the critical current density reduces to almost zero in the warm part of the sample during the short period of non-equilibrium. A peak trapped field of 4.1 T at the surface and 5.3 T between a stack of two GdBCO–Ag bulk superconductors was achieved at 30 K by means of an optimised two-step pulse sequence with the assistance of the flux jumps, which is extremely promising for potential applications of these technologically important materials.

Keywords: bulk superconductor, superconducting magnet, flux jump, magnetisation

(Some figures may appear in colour only in the online journal)

Introduction

Large, single grain (RE)-Ba–Cu–O [(RE)BCO, where RE is a rare-earth element or Y] bulk high temperature superconducting (HTS) materials can potentially be used to improve the performance of a range of engineering applications, such as superconducting bearings, flywheel energy storage systems, rotating machines and non-contact mixers [1–6]. This is due, primarily, to their ability to trap magnetic fields that are significantly greater than those produced by conventional, iron-based permanent magnets. Indeed, a trapped magnetic field of 17.6 T at 26 K, reported in 2014 in a stack of two, Ag-containing $GdBa_2Cu_3O_{7-\delta}$ (GdBCO) bulk superconductors [7], underlines the potential of these materials for practical applications. However, magnetisation is one of the main barriers to practical use of bulk superconductors as high field pseudo-permanent magnets. Recently several

[3] Author to whom any correspondence should be addressed.

authors have reported a flux jump phenomenon that enables efficient magnetisation at lower fields than would be predicted on the basis of the Bean model using the pulsed field magnetisation (PFM) technique [8–10].

Magnetic flux jumps which are a common phenomenon in type II superconductors, often present a significant challenge to the development of practical applications of these materials. Wipf described flux jumps as a runaway process initiated by a small fluctuation of the external magnetic field or temperature, manifesting itself as an avalanche-like migration of magnetic flux into or out of the volume of the superconductor [11]. It is possible to use magneto-optical imaging to visualise the avalanche process, which provides clear experimental basis for this observation [12, 13]. During a flux avalanche, the critical current density, J_c, is reduced dramatically due to a rise in sample temperature during the flux jump process, which, in turn, causes a reduction in the screening current to such an extent that the external field can no longer be shielded from the interior of the sample. The superconductor is consequently in a non-equilibrium state during a flux jump and a theory to describe comprehensively the dynamic characteristics of the magnetic flux, and thus J_c during this process, has yet to be developed. The solution to this problem is likely to involve multiple flux pinning mechanisms [14, 15], and is of great relevance to understanding both the fundamental physics and applied properties of bulk superconductors. The flux jump phenomenon has been observed and studied in both conventional type II superconductors and in high temperature superconductors [16, 17] primarily via non-contact magnetisation measurements. However, flux jumps, as reported by Müller *et al* have been observed only at temperatures below 7.6 K, in hysteresis loops of melt-textured $YBa_2Cu_3O_{7-\delta}$ (YBCO) [16]. The occurrence of flux jumps is related closely to the sweep rate of the external field [13, 18].

Flux jumps are generally thought of as a hazard that lead commonly to the quench of superconducting magnets, and, as far as possible, are designed out in practical applications. It is pleasing to be able to report that for the conditions discussed in this work, flux jumps can be used to assist the penetration of magnetic flux into bulk superconductors in the PFM process. In PFM, flux jumps minimise the shielding effect of the induced supercurrent and reduce significantly the magnitude of applied magnetic field (B_a) required to achieve a target trapped field [8–10, 19–21], analogous to a process that is closer to field cooling (FC). In this paper, we report flux jumps in bulk HTS observed during a PFM process with a pulsed magnetic field of up to 7 T and a fixed rise time of 35 ms. The flux jumps were studied using cylindrical GdBCO samples of 30 mm diameter with a view to developing a practical magnetisation process for high field applications, in general.

Instability criterion for flux jumps

The criterion for the occurrence of flux jumps, which is based on the assumption that the thermal diffusivity of the material is much smaller than its electromagnetic diffusivity, is appropriate for PFM which has, in general, an extremely short time duration. This means that any heat generated due to the movement of magnetic flux cannot be removed quickly from the sample by cooling and, as such, the problem can be simplified by assuming the process is adiabatic. A theory was proposed on this basis by Wipf [22] and by Swarts and Bean [23] based fundamentally on the critical state model. The theory assumed a sample of infinite slab geometry in the superconducting state and subject to an external field, B_a, with a field penetration depth given by $a = B_a/\mu_0 J_c$. The total flux in the superconductor changes when the applied field is increased by a small amount, ΔB_a, by $\Delta\Phi = \frac{1}{2}\Delta B_a \cdot a = \frac{\Delta B_a \cdot B_a}{2\mu_0 J_c}$, which results in a dissipation of heat equal to $\Delta Q = \Delta\Phi \cdot J_c$. The effect of this is to diminish J_c by $\Delta J_c = \frac{\Delta Q}{C}\frac{dJ_c}{dT}$, where C is the specific heat capacity of the superconductor. Consequently, the field shielding ability of the sample is reduced by $\Delta B_{sh} = \mu_0 \Delta J_c a$. A flux jump is then triggered if $\Delta B_{sh} \geqslant \Delta B_a$. In this case, the instability field for the flux jump is given straightforwardly by the following equation using $\Delta B_{sh} = \Delta B_a$ as a critical condition,

$$B_j = \sqrt{\frac{2\mu_0 C J_c}{-dJ_c/dT}}. \quad (1)$$

The same formula can be deduced if the origin of disturbance is due to temperature rather than applied field. J_c is reduced by $\Delta J_c = T_1\, dJ_c/dT$ when temperature is increased by ΔT_1, which leads to the dissipation of heat and raises the temperature by ΔT_2. A flux jump will be triggered if the temperature rise is not convergent, which means $\Delta T_2 > \Delta T_1$.

Mints calculated the heat dissipation as $Q = \int \boldsymbol{J} \cdot \boldsymbol{E} dx$ by introducing the conductivity σ from the E–J power law, $E/E_0 = (J/J_c)^n$, into the formulation [18]. This is closely related to the ramp rate $\dot{\boldsymbol{B}}_a$ of the applied field given that $\nabla \times \boldsymbol{E} = -d\boldsymbol{B}_a/dt$. Mints gives the following expression for the flux jump field using the J_c (B, T) relationship, where $J_c(B) = \alpha(T)/B$ is given by the Kim–Anderson model

$$B_j = \left[\frac{2\mu_0^2 \alpha(T_0) h (T_c - T_0)}{n\dot{B}_a}\right]^{1/3}. \quad (2)$$

Here h is the heat transfer coefficient to the coolant at ambient temperature T_0.

This instability criterion predicts when a flux jump will happen based on the thermodynamic conditions of the material. The superconductor enters a highly non-equilibrium state during a flux jump, however, where J_c (B, T) can no longer be derived from the critical state by the balance of the Lorentz and flux pinning forces or the Bean model. As a result, a parameter α ($0 \leqslant \alpha \leqslant 1$), defined by the ratio of J_c during and before the flux jump, has been proposed in previous studies to quantify the magnetisation or 'size' of the flux jump [24, 25]. It is possible to inversely deduce α and thus J_c in the non-equilibrium state according to the flux jumps in the hysteresis loops [16]. Romero-Salazar *et al* [24] simulated flux jumps in hysteresis curves of MgB_2 and achieved good agreement with theory using the instability

criterion. They reported that the ratio α should be selected carefully based on specific experimental conditions, which include temperature, the magnetic history of the superconductor and the specific quadrant of the hysteresis curve. This study showed, for example, the first flux jump in the virgin curve, where B_a increases from 0 T, at 5 K is independent of the value of α. However, the second flux jump then occurs at the B_a measured experimentally only when $\alpha = 0.025$, which indicates that the remnant magnetisation influences the instability. This is important in the optimisation of a multi-pulse magnetisation procedure such as that studied here [26, 27].

Zhou *et al* [28] simulated numerically the flux jumps in a hysteresis loop reported in [17]. The results obtained are in good agreement with experiment when the B_j predicted by equation (1) is one order of magnitude smaller than the experimental data and the B_j given by equation (2) is larger by a factor of two. These results are based on modification of the E–J relationship and the addition of the thermal transient equation to the model, which was then solved via a finite difference method (FDM). These authors reported that J_c was reduced by five to six orders of magnitude at each jump, accompanied by a sudden rise in temperature.

More recently, Ainslie *et al* [29] reproduced the flux jumps during a PFM process in a well-developed 2D axisymmetric model using the finite element method (FEM). One concern, however, is how to translate the discontinuity of J_c in the magnetisation curve. In general, J_c, as defined by the J_c (B, T) relationship, is a continuous variable unless B_a exceeds the irreversibility field or T exceeds the critical temperature, T_c, which, for example, is frequently the case for MgB_2 [30–32]. However, this is an unlikely case for HTS materials due to their higher T_c, J_c and irreversibility field and lower thermal conductivity at typical operating temperatures. The discontinuity associated with a flux jump may be introduced at the boundary of the elements in the FDM or FEM, which appears physically reasonable given that flux jumps originate predominantly at hot spots associated with the localised generation of heat. In the present study, the instability criterion to address specifically the discontinuity in J_c. We extend the instability criterion in a 2D axisymmetric model using experimental data, including a realistic J_c (B, T), to re-calculate B_j and compare the outcome with the results of the PFM experiments.

Experimental details

GdBCO bulk superconductors, containing 10% Ag by weight, of diameter 30 mm and thickness 12 mm were prepared by a standard top seeded melt growth technique [33, 34]. The trapped field performance of these samples was evaluated following field cooled magnetisation at 77 K. The peak magnetic flux density on the surface of the large single grains, on average, exceeded 1 T. The observed trapped field distribution of each single grain sample exhibited good homogeneity, as shown in figure 1(c), which generally suggests a high-quality sample. Each sample was cooled

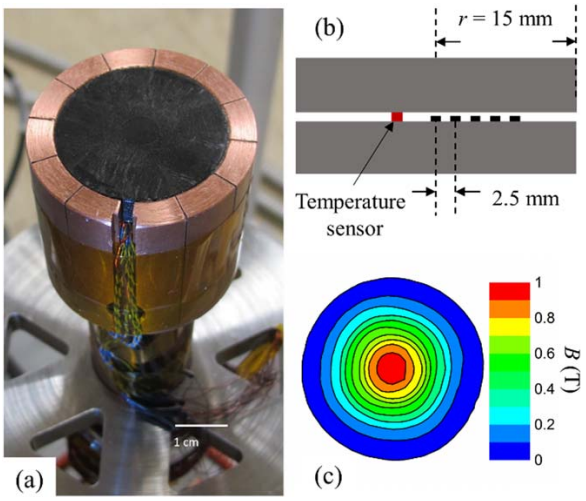

Figure 1. (a) Photograph of a stack of two single grain GdBCO–Ag bulk superconductors encapsulated in a slotted copper holder, which is connected to the cold-finger of the cyrocooler. (b) The arrangement of the array of five Hall sensors and Cernox temperature sensor. (c) Trapped field distribution of the GdBCO–Ag sample measured after field cooled magnetisation at 77 K.

conductively using a GM cryo-cooler, illustrated in figure 1(a), with a base temperature of 17 K. The temperature was monitored and controlled throughout the cooling and measurement process by means of a Cernox temperature sensor coupled to a heater. The local magnetic flux density was measured directly using an array of five calibrated Hall sensors separated by 2.5 mm to obtain a field profile from the centre to the edge of the sample. Data were collected during the entire PFM process with a sampling rate of 2 kHz. The sample was then cut in half to form a stack of two independent discs, and the measurements were repeated with the Hall sensors re-positioned at the centre of the stack (i.e. along the radius between the two discs), as shown in figure 1(b). An additional Cernox temperature sensor was placed in contact with the sample in the new arrangement to measure the temperature rise during the PFM process.

The pulsed magnetic field was provided by discharging a capacitor bank through a copper solenoid immersed in liquid nitrogen. The rise time of the pulse, shown in figure 2, was 35 ms for a quarter cycle of a sine wave (the RLC circuit had an under-damped response). The charging circuit was opened when the current reached its peak value, with the return current flowing through a fly-back diode and reducing to zero in about 450 ms. On this basis, the pulsed field can be expressed as

$$B_a = \begin{cases} B_{a,peak} \sin \frac{2\pi}{35 \times 4} t & (t \leqslant 35 \text{ ms}) \\ B_{a,peak} e^{-\frac{t-35}{0.104}} & (t > 35 \text{ ms}) \end{cases} . \quad (3)$$

This expression for applied field was used for all the subsequent simulations undertaken as part of this study.

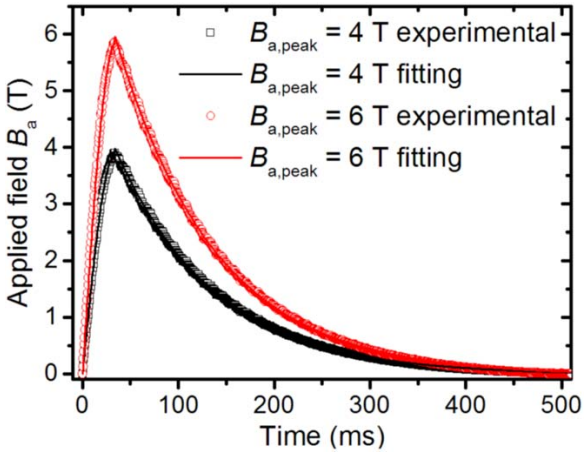

Figure 2. Profile of applied fields of magnitude of 4 and 6 T. The solid lines are fits to the experimental curves using equation (3). The rise time of the pulse is 35 ms over a quarter cycle of a sine wave, and the fall time is approximately 450 ms.

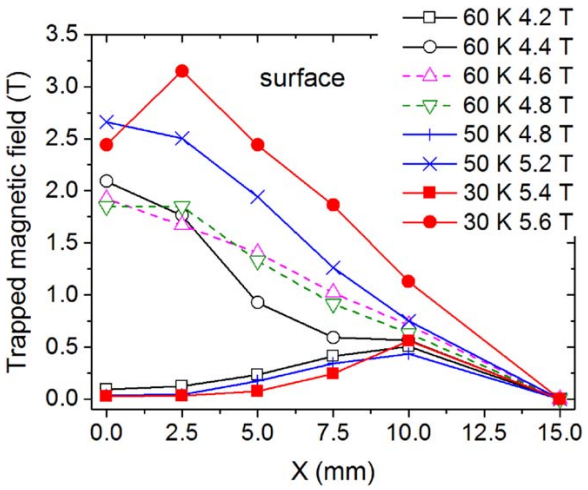

Figure 3. Trapped field profile measured above the surface of the GdBCO–Ag bulk superconductor 15 min after the PFM process, for different applied fields, B_a, at temperatures of 30, 50 and 60 K.

Modelling framework

A standard 2D axisymmetric model, described in [29, 35–38] was used in this study, which is based on the $\boldsymbol{H}$-formulation with the following governing equations (Faraday's and Ampere's laws)

$$\begin{cases} \nabla \times \boldsymbol{E} = -\dfrac{d\mu_0\mu_r \boldsymbol{H}}{dt} \\ \nabla \times \boldsymbol{H} = \boldsymbol{J} \end{cases}. \tag{4}$$

These are coupled with the thermal transient equation,

$$\rho \cdot C\frac{dT}{dt} = \nabla \cdot (k\nabla T) + Q. \tag{5}$$

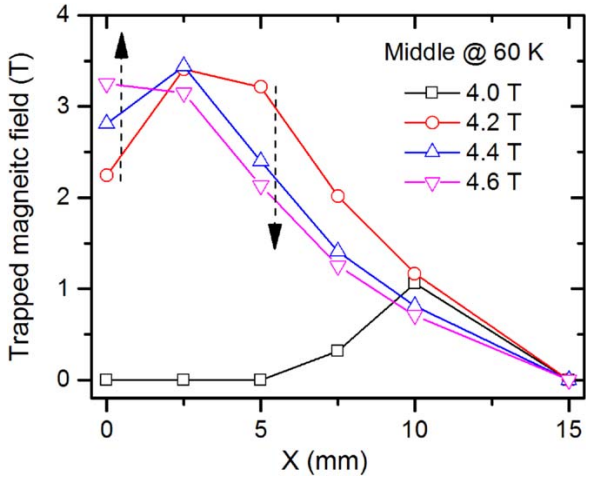

Figure 4. Trapped field measured between the stack of two GdBCO–Ag bulk superconductors after PFM at 60 K.

The simulation was implemented using the commercial FEM software package COMSOL Multiphysics. A relative permeability, $\mu_r = 1$ was assumed for the superconductor, and its electrical properties were modelled using the E–J power law, $E \propto J^n$, where $n = 20$. In this case, the resistivity of the superconductor ρ_{sc} is equal to

$$\rho_{sc} = \frac{E_c}{J_c}\left|\frac{J}{J_c}\right|^{n-1}, \tag{6}$$

where the characteristic electric field $E_c = 10^{-4}\,\mathrm{V\,m^{-1}}$. The resistivity is modified to include the flux flow region regarding the rapidly changing external field as follows,

$$\rho = \frac{\rho_{sc} \cdot \rho_{normal}}{\rho_{sc} + \rho_{normal}}. \tag{7}$$

In this case, the resistivity tends towards a normal state value, $\rho_{normal} = 3.5 \times 10^{-6}\,\Omega\,\mathrm{m}$, when the induced electrical field E significantly exceeds E_c. The key parameter J_c (B, T) for the model was obtained directly via a two-variable interpolation from the $J_c(B)$ curves calculated from magnetisation loops measured between 30 to 85 K and up to 6 T using a SQUID magnetometer, which was further extended mathematically up to 10 T, as described in [29, 35]. The heat source, Q, was calculated as $Q = \boldsymbol{E} \cdot \boldsymbol{J}$.

Results and discussion

B_j measured experimentally

Figure 3 shows the profile of the trapped field measured 15 min after the PFM process at different temperatures to allow for flux creep. Taking the 60 K results as an example, the trapped field profile exhibits a trough-like, half 'M' shape distribution when B_a is 4.2 T. However, when the applied field is increased by only 0.2 T to $B_a = 4.4$ T, the trapped field profile changes to a peak distribution with a maximum peak flux density of

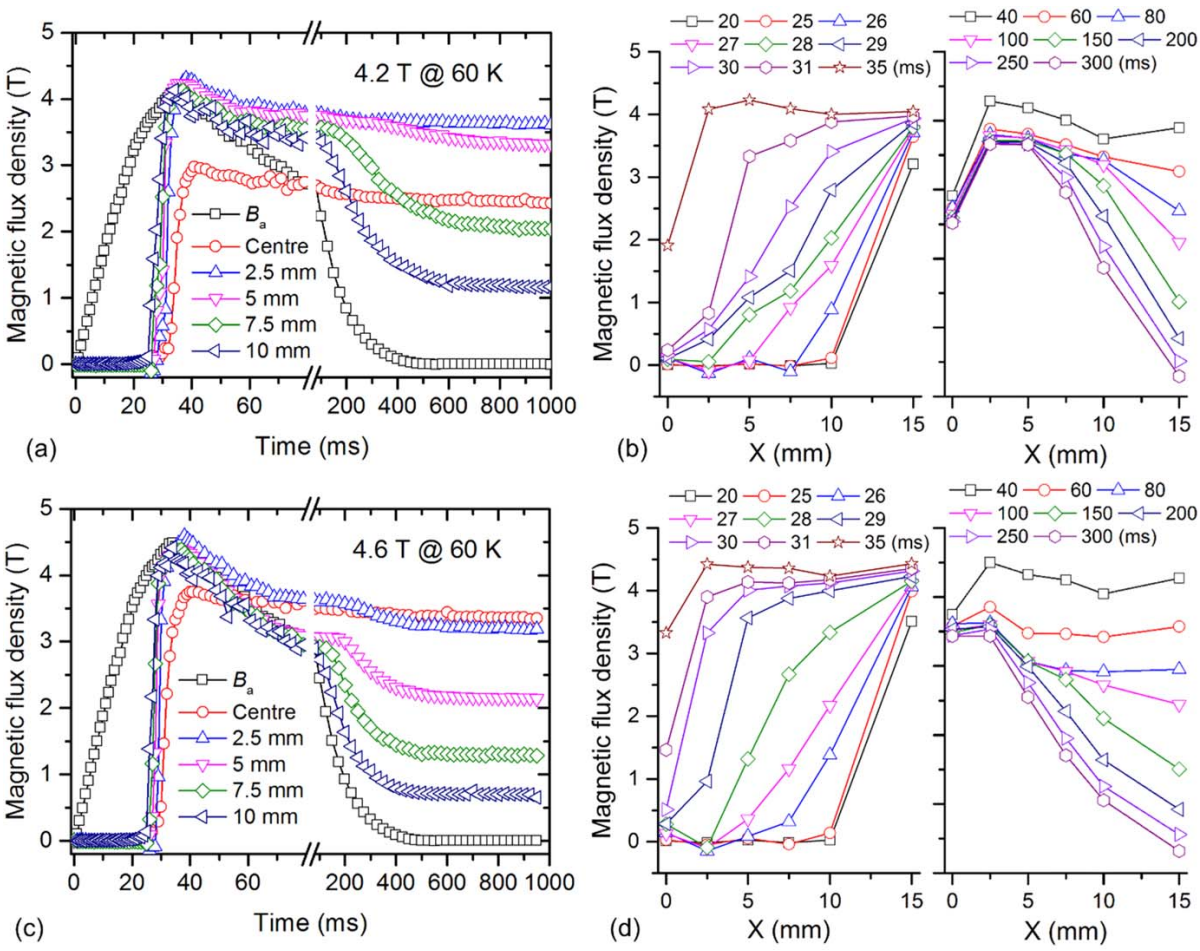

Figure 5. Measured magnetic field at different positions in the stack of two GdBCO–Ag discs for applied field $B_a = 4.2$ T at 60 K. (a) Measured magnetic field as a function of time during the entire PFM process, and (b) field distribution at different times during the rise and fall of the applied field. (c) and (d) correspond to the case where $B_a = 4.6$ T at 60 K.

2.1 T at 60 K. Increasing the applied field further to 4.6 and 4.8 T decreases the peak flux density monotonically due to excessive generation of heat. The critical applied field, $B_a = 4.4$ T, is therefore defined as B_j at 60 K. The measured B_j was observed to be consistent in repeated experiments and to increase with decreasing operating temperature.

The Hall sensors measure only the perpendicular component of the magnetic field. In order to minimise the transverse field component, the magnetic field was also measured by Hall probes sandwiched between the stack of two GdBCO–Ag discs, as shown in figure 4. The observed critical field, B_j, in the two-sample stack was 4.2 T which was approximately 0.2 T smaller than that measured for the single domain. The incorporation of the Hall sensors within the bulk superconductor stack introduces a gap of 2 mm which will affect the behaviour of the magnetic field to penetrate the samples. And the process of splitting the bulk superconductor may cause a slight degradation of its properties. The peak in the trapped field profile for this arrangement was off-centre, which differed from that measured at the top surface of the sample. This indicates that the magnetic flux actually did not jump all the way to the centre of the sample. Flux was pushed further towards the centre when magnetic fields higher than 4.2 T were applied, which enhanced the peak flux density, but reduced the trapped field towards the edge of the sample as indicated by the dashed arrows in figure 4.

The local flux density was recorded at different radial positions during the entire PFM process to obtain a better understanding of the flux penetration dynamics within the bulk superconductor. Figure 5 shows the measured magnetic field at 60 K and applied fields of $B_a = 4.2$ T, which is the flux jump field, B_j, and $B_a = 4.6$ T. It can be seen from figure 5(a) that a flux jump occurs when the external field approaches B_j, and that it is shielded perfectly by the induced current prior to the occurrence of flux jump. However, the measured field rises sharply once the flux jump has occurred and becomes equal to the applied field at a position of 2.5 mm from the centre of the sample. This indicates that the induced shielding current, and thus J_c at the outer portion of the sample, has decreased to zero which means this part of the sample is in the flux flow state.

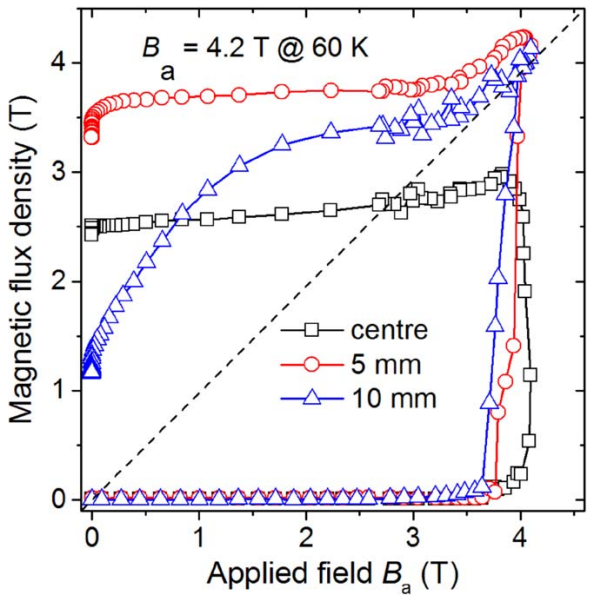

Figure 6. Local magnetic field measured at $r = 0$, 5 and 10 mm from the centre inside the two-disc GdBCO–Ag stack as a function of applied field for the case where $B_a = 4.2$ T at 60 K.

The variation of the field profile in such a relatively large sample, illustrated in figure 5(b), enables a closer examination of the flux penetration front. The magnetic field distribution follows the critical state model, with the gradient of the flux density being directly proportional to J_c of the sample, until a flux jump occurs at 31 ms. The magnetic field, assisted by the flux jump, fully penetrates to around 2.5 mm from the centre of the sample. It is worth noting that the flux creep at the outer portion of the sample is much more severe during and following the removal of the external field, and that the magnetic flux that 'jumps' in during the PFM process remains stable. It can be seen by comparing the results for applied fields B_a of 4.2 and 4.6 T that the flux jump occurs earlier (at around 29 ms) and that a greater amount of flux penetrates to the centre of the sample for B_a of 4.6 T. In addition, more flux exits the sample from its periphery due to flux creep during the period over which B_a decreases to zero for $B_a = 4.6$ T. These observations are consistent with the measured final trapped field shown in figure 4.

Figure 6 shows the measured magnetic field as a function of applied field for $B_a = 4.2$ T at 60 K. The curves appear similar to *M–H* hysteresis loops, and the flux jump can be observed clearly at the point where the measured field at 5 and 10 mm from the centre of the sample increases in magnitude from zero to a value equal to the external field.

B_j obtained by the numerical method

It is apparent from the preceding discussion that the flux jump instability is triggered at the point where the shielding field (i.e., the magnetic field generated by the induced screening

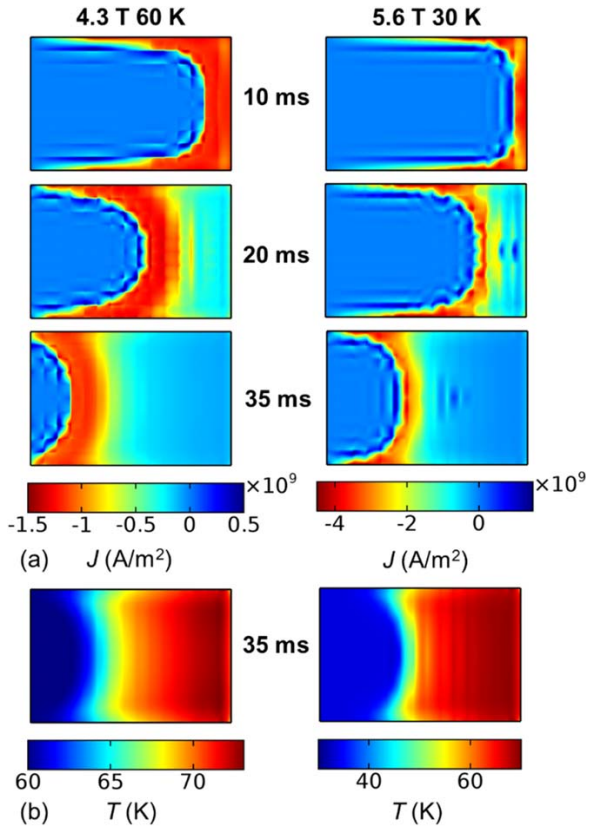

Figure 7. (a) Magnitude and distribution of the induced current density, *J*, flowing in the cross section of the bulk superconductor at times $t = 10$, 20 and 35 ms for $B_a = 4.3$ T at 60 K (left) and $B_a = 5.6$ T at 30 K (right). (b) Temperature distribution at $t = 35$ ms (peak of the applied field) for $B_a = 4.3$ T at 60 K (left) and $B_a = 5.6$ T at 30 K (right).

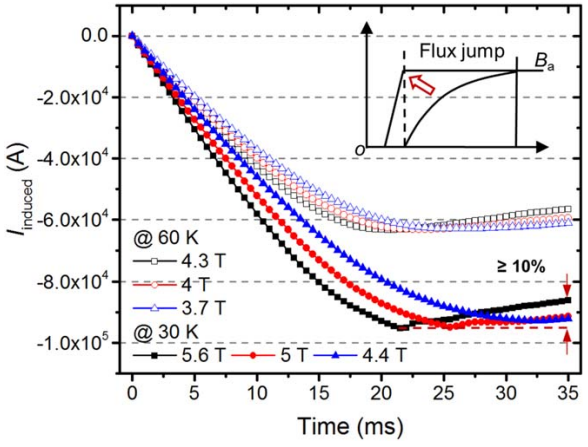

Figure 8. Calculated induced current, $I_{induced}$, during the rise of the pulsed field at 60 and 30 K. The inset illustrates the process of the triggering of an instability and the reconstruction of a critical state at the penetration front.

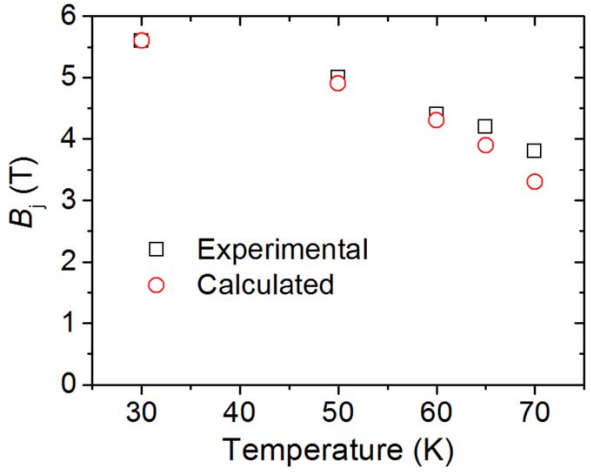

Figure 9. Critical applied field, B_j, triggering the flux jump, obtained from experiments and simulations at different temperatures for the GdBCO–Ag single grain sample.

current) starts to decrease while the external field is still increasing. At this point, the forces on flux lines that were previously pinned can no longer be resisted, and the critical state breaks down. In the 2D axisymmetric model, the induced current, I_{induced} in the bulk superconductor can be expressed as the current density, J, flowing around the bulk superconductor, integrated over the cross section of the sample (i.e., radius × thickness),

$$I_{\text{induced}} = \int_s J \cdot ds. \tag{8}$$

Figure 7(a) shows the distribution of the induced current density, J, for the cases of $B_a = 4.3$ T at 60 K (left) and $B_a = 5.6$ T at 30 K (right). I_{induced} increases with the increase of the penetration region during the rise of the external field. However, the induced current decreases synchronously due to the generation of heat, which reduces J_c, and subsequently J. The decrease in J is significant, as illustrated in figure 7(a), due to the dramatic temperature rise as shown in figure 7(b). The heat capacity, C, of GdBCO is very small at low temperatures and increases rapidly with increasing temperature. The magnitude of C at 30 K is approximately 56 times larger than its value at 4 K in the model parameters used for simulation [36]. Therefore, the change of temperature, and hence J_c of the superconductor, for a given amount of heat generated due to flux motion reduces significantly at higher operating temperatures. This explains both why flux jumps are observed only at temperatures below 7.6 K in the magnetometry measurements performed on a YBCO sample in [16] and why they are less problematic for HTS materials at elevated temperatures. In PFM, however, the rapid change of the external field, especially during the rise of the pulsed field increases significantly the amount of heat generated in the superconductor, which facilitates the occurrence of flux jumps.

Figure 8 shows the change of induced current during the increase in pulsed field. At 30 K, for example, when $B_a =$ 4.4 T, the current increases with increasing applied field and

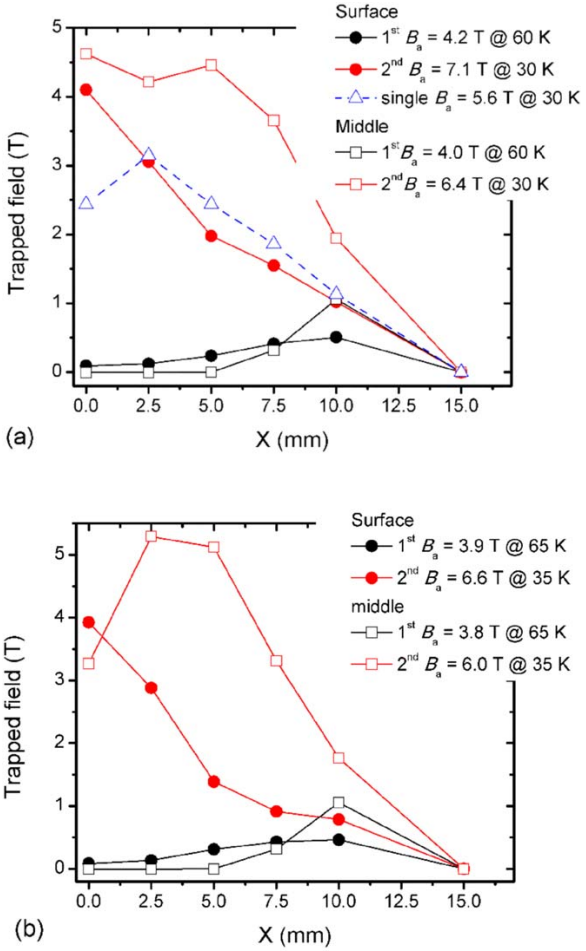

Figure 10. Trapped field profile achieved using the two-temperature, multi-pulse magnetisation (MPFM) method with temperature sequences of 60–30 K (a) and 65–35 K (b). The measurements were performed at the surface and in the middle of the two-sample GdBCO–Ag stack. The sigle pulse result for $B_a = 5.6$ T at 30 K was included for reference.

reaches a maximum value when B_a approaches its peak. When B_a is increased to 5.6 T, the maximum value of induced current appears after approximately 22 ms and starts to decrease afterwards due to the severe generation of heat. This represents the point at which the shielding current is unable to exclude the external field, as described by the instability criterion. B_j is then defined as the value of B_a that reduces the induced current by 10% of its maximum value at the end of the field rise period of the PFM process. The values of B_j determined at different temperatures by the numerical methods, shown in figure 9, are in good agreement with the experimental data derived from figure 3. The ramp rate of the external field, dB_a/dt, is determined by the magnitude of B_a given that the time duration of the PFM process is a constant. Therefore, B_j is influenced by both the magnitude and ramp rate of the applied field.

A critical state, as illustrated schematically in the inset of figure 8, will be re-established at the penetration front

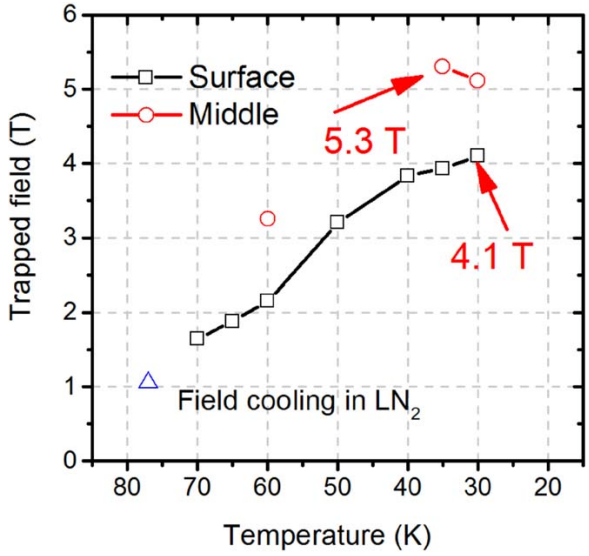

Figure 11. Maximum magnetic flux densities achieved at different temperatures at the surface and in the middle of the two-sample GdBCO–Ag stack of diameter 30 mm via single PFM ($\geqslant$60 K) and MPFM ($<$60 K, corresponding to the operating temperature of the second pulse).

following the flux jump. The flux jump occurs within the penetration area of the sample where most of the heat has been generated (i.e., the 'warm region'), which explains why the peak trapped field appears further away from the sample centre at lower temperatures, where the penetration area is smaller due to a higher J_c, as shown in figures 3 and 4. Hence, the value of J_c in the warm region during the flux jump is critical to the process. J_c in the model is continuous, although the average J_c decreases dramatically to approximately 40% of its original value at $t = 35$ ms. However, the experimental results shown in figures 5 and 6, indicate that J_c decreases entirely to zero in the outer portion of the sample, since the measured magnetic field in these regions is equal to the applied field.

It is worth noting that B_a observed both experimentally and predicted by the model is smaller than the full penetration field B^*. The induced current will decrease monotonically with decreasing J_c once B_a reaches B^*. After that the penetration area becomes stable, suggesting that a flux jump is likely to happen when $B_a \geqslant B^*$, which is consistent with considerations of the effect of sample size on the probability of flux jumps [28].

Multi-pulse magnetisation

The accumulated, localised heat is directly responsible for producing the flux jump in the model presented here. The flux jump initiates in the field penetration area which decreases in size at lower temperatures due to stronger pinning forces (and hence higher J_c). This hypothesis has been used to develop a two-temperature, multi-pulse magnetisation (MPFM) method, in which a field slightly smaller than B_j is applied to the superconductor at temperature T_1, to partially magnetise the sample, followed by the application of a higher field at T_2, where $T_2 < T_1$. As a result, some flux is pinned in the superconductor by the application of the first pulse in an attempt to reduce the heat generated during the field penetration in the second pulse [39], consequently triggering the flux jump at a higher B_a and at a position closer to the centre of the sample.

Figure 10 shows the results of a two-temperature MPFM process with temperature sequences of $T_1 = 60$ K to $T_2 = 30$ K (a) and $T_1 = 65$ K to $T_2 = 35$ K (b). As is expected for the MPFM method, the peak magnetic flux density at the surface of the sample, shown in figure 10(a), reaches 4.1 T at 30 K with the peak at its centre. This is in contrast with the peak magnetic flux density of 3.2 T achieved from a single-pulse where the peak position is 2.5 mm away from the centre of the sample, as shown in figure 3. Significantly, the value of B_j at 30 K increases from 5.6 T for the single-pulse magnetisation process to 7.1 T for MPFM. This confirms that an applied field of greater magnitude is required for the subsequent pulse in the MPFM process, as reported in [39]. The same temperature sequence was used for the stack of two GdBCO–Ag discs. The trapped field profile, as shown in figure 10(a), reveals clearly that the flux has not yet completely 'jumped' to the centre of the sample.

Trapped field profiles achieved using a temperature sequence of $T_1 = 65$ K to $T_2 = 35$ K are shown in figure 10(b). The peak trapped field is 3.9 T at the surface of the single domain and 5.3 T in the middle of the two-sample stack. This indicates that reducing the operating temperature in PFM is not always efficient for enhancing the trapped magnetic field. A greater temperature rise of the sample is observed due to the smaller heat capacitance and increased generation of heat at lower operating temperatures. An optimal operating temperature, therefore, exists for the PFM process.

Figure 11 summaries the maximum trapped field achieved in the present study at different temperatures. The MPFM method is applicable when the temperature is below 60 K, and had been used to generate a maximum peak flux density of 4.1 T at the surface and 5.3 T at the centre of a GdBCO–Ag single grain of diameter 30 mm.

Conclusions

Flux jumps in a single grain GdBCO–Ag bulk superconductor of diameter up to 30 mm have been observed during the PFM process. The critical applied field required to trigger the flux jump, B_j, at different temperatures has been determined. An instability criterion has been proposed based on a 2D axisymmetric finite element to enable the occurrence of flux jumps to be predicted. The value of B_j obtained numerically using this criterion agrees well with the results of experiment.

We conclude that accumulated heat during the magnetic field penetration is the dominant factor that leads directly to the flux jump. The 'warm area' where the flux jump occurs, which is predicted successfully by the model, explains why at lower temperatures the flux jump happens only partially in the

outer portion of the sample. The experimental results reveal that J_c in the 'warm area' is approximately zero during the flux jump itself.

The results of this investigation have been used to further refine the PFM approach and to develop a multi-pulse magnetisation technique, which has been used to achieve trapped field with peak value of 4.1 T at the surface and 5.3 T inside a GdBCO–Ag sample. This is a significant step towards achieving higher trapped fields in bulk superconducting magnets, magnetised by the PFM technique, towards utilising these materials practically in range of engineering applications.

Acknowledgments

This work was supported by the Siemens Company and by the Engineering and Physical Sciences Research Council (grant number: EP/P00962X/1). Mark Ainslie would like to acknowledge financial support from an Engineering and Physical Sciences Research Council (EPSRC) Early Career Fellowship EP/P020313/1. We are particularly grateful to Professor Fujishiro of Iwate University for useful discussions. Data related to this publication are available at the University of Cambridge data repository https://doi.org/10.17863/CAM.23697.

ORCID iDs

Difan Zhou https://orcid.org/0000-0001-9889-8872
Mark D Ainslie https://orcid.org/0000-0003-0466-3680
Jan Srpčič https://orcid.org/0000-0001-8195-4188
Yunhua Shi https://orcid.org/0000-0003-4240-5543
David A Cardwell https://orcid.org/0000-0002-2020-2131
John H Durrell https://orcid.org/0000-0003-0712-3102
Martin Boll https://orcid.org/0000-0002-9778-4280

References

[1] Campbell A M and Cardwell D A 1997 *Cryogenics* **37** 567–75
[2] Hull J R 2000 *Supercond. Sci. Technol.* **18** R1–15
[3] Werfel F N, Floegel-Delor U, Riedel T, Rothfeld R, Wippich D, Goebel B, Reiner G and Wehlau N 2007 *IEEE Trans. Appl. Supercond.* **17** 2138–41
[4] Zhou D, Izumi M, Miki M, Felder B, Ida T and Kitano M 2012 *Supercond. Sci. Technol.* **25** 103001
[5] Watasaki M, Miki M, Felder B, Tsuzuki K, Sato R, Kase S, Izumi M and Ida T 2013 *IEEE Trans. Appl. Supercond.* **23** 8201604
[6] Koyama F, Akiyama S and Murakami M 2006 *Supercond. Sci. Technol.* **19** S572–4
[7] Durrell J H *et al* 2014 *Supercond. Sci. Technol.* **27** 082001
[8] Weinstein R, Parks D, Sawh R-P, Carpenter K and Davey K 2015 *Appl. Phys. Lett.* **107** 152601
[9] Weinstein R, Parks D, Sawh R-P, Carpenter K and Davey K 2016 *J. Appl. Phys. Lett.* **119** 133906
[10] Zhou D, Ainslie M D, Shi Y, Dennis A R, Huang K, Hull J R, Cardwell D A and Durrell J H 2017 *Appl. Phys. Lett.* **110** 062601
[11] Wipf S L 1991 *Cryogenics* **31** 936
[12] Altshuler E and Johansen T H 2004 *Rev. Mod. Phys.* **76** 471
[13] Baruch-El E, Baziljevich M, Shapiro B Y, Johansen T H, Shaulov A and Yeshurun Y 2016 *Phys. Rev.* B **94** 054509
[14] Campbell A M and Evetts J E 1972 *Adv. Phys.* **21** 199–428
[15] Blatter G, Feigel'man M V, Geshkenbein V B, Larkin A I and Vinokur V M 1994 *Rev. Mod. Phys.* **66** 1125
[16] Müller K-H and Andrikidis C 1994 *Phys. Rev.* B **49** 1294
[17] Nabialek A, Niewczas M, Dabkowska H, Dabkowski A, Castellan J P and Gaulin B D 2003 *Phys. Rev.* B **67** 024518
[18] Mints R 1996 *Phys. Rev.* B **53** 12311
[19] Fujishiro H, Tateiwa T, Fujiwara A, Oka T and Hayashi H 2006 *Physica* C **445** 334
[20] Yanagi Y, Itoh Y, Yoshikawa M, Oka T and Mizutani U 2005 *Supercond. Sci. Technol.* **18** 839
[21] Fujishiro H, Yokoyama K, Kaneyama M, Ikebe M, Oka T and Noto K 2005 *Physica* C **426–431** 594–601
[22] Wipf S L 1967 *Phys. Rev.* **161** 404
[23] Swartz P S and Bean C P 1968 *J. Appl. Phys.* **39** 4991
[24] Romero-Salazar C, Morales F, Escudero R, Durán A and Hernández-Flores O A 2007 *Phys. Rev.* B **76** 104521
[25] Chabanenko V V, D'yachenko A I, Chabanenko A V, Zalutsky M V, Szymczak H, Piechota S and Nabialek A 1998 *Supercond. Sci. Technol.* **11** 1181
[26] Fujishiro H, Kaneyama M, Tateiwa T and Oka T 2005 *Japan. J. Appl. Phys.* **44** L1221
[27] Fujishiro H, Hiyama T, Naito T, Yanagi Y and Itoh Y 2009 *Supercond. Sci. Technol.* **22** 095006
[28] Zhou Y and Yang X 2006 *Phys. Rev.* B **74** 054507
[29] Ainslie M D, Zhou D, Fujishiro H, Takahashi K, Shi Y and Durrell J 2016 *Supercond. Sci. Technol.* **29** 124004
[30] Xia J, Li M and Zhou Y 2017 *Supercond. Sci. Technol.* **30** 075004
[31] Fujishiro H, Mochizuki H, Naito T, Ainslie M D and Giunchi G 2016 *Supercond. Sci. Technol.* **29** 034006
[32] Fujishiro H, Mochizuki H, Ainslie M D and Naito T 2016 *Supercond. Sci. Technol.* **29** 084001
[33] Shi Y, Namburi D K, Zhao W, Durrell J H, Dennis A R and Cardwell D A 2016 *Supercond. Sci. Technol.* **29** 015010
[34] Zhou D, Hara S, Li B, Xu K, Noudem J and Izumi M 2013 *Supercond. Sci. Technol.* **26** 015003
[35] Ainslie M D and Fujishiro H 2015 *Supercond. Sci. Technol.* **28** 053002
[36] Ainslie M D, Fujishiro H, Mochizuki H, Takahashi K, Shi Y, Namubri D K, Zou J, Zhou D, Dennis A R and Cardwell D A 2016 *Supercond. Sci. Technol.* **29** 074003
[37] Ainslie M D, Zou J, Mochizuki H, Fujishiro H, Shi Y, Dennis A R and Cardwell D A 2015 *Supercond. Sci. Technol.* **28** 125002
[38] Ainslie M D, Fujishiro H, Ujiie T, Zou J, Dennis A R, Shi Y and Cardwell D A 2014 *Supercond. Sci. Technol.* **27** 065008
[39] Ainslie M D, Srpčič J, Zhou D, Fujishiro H, Takahashi K, Cardwell D and Durrell J H 2018 *IEEE Trans. Appl. Supercond.* **28** 6800207